Supporting information for "Dynamic Inhomogeneity in the Photodynamics of the Cyanobacterial Phytochrome Cph1Δ"

Peter W. Kim,[†] Nathan C. Rockwell,[‡] Shelley S. Martin,[‡] J. Clark Lagarias,[‡] Delmar S. Larsen[*,†]

[†]Department of Chemistry and [‡]Department of Molecular Cellular Biology, University of California at Davis, One Shield Avenue, Davis, CA, 95616

Global Analysis

Global analysis technique[1, 2] has been successfully applied to phytochrome-related systems to characterize their initial photodynamics, and the details of the technique and analysis are included with these studies.[3-6] A multi-compartment global analysis formalism fits the data to an underlying "target" model with time-dependent populations (i.e., concentration profiles) with time-independent spectra. This is accomplished by fitting the data with numerical solutions of linear first-order differential equations describing a postulated model (Eq. 1):

$$\frac{dn_i}{dt} = A_i I(t) + \sum_j K_{ij} n_j \qquad (1)$$

In Equation 1, n_i represents the i^{th} microscopic population of interest, A_i is the initial occupancy of i^{th} excited state, I(t) is the pump pulse temporal envelope, and K_{ij} are the rate constants describing the *exponential* flow from one population into another. If the underlying target model accurately describes the dynamics, the extracted spectra from the analysis are termed Species Associated Difference Spectra (SADS) and represent the true difference spectra of the constituent populations. If the model inaccurately describes the dynamics, the resulting spectra from the global fitting are Evolution Associated Difference Spectra (EADS) and are linear combinations of the underlying SADS. In the next section, the details of kinetic model construction for temperature-dependent and excitation wavelength-dependent signals of Cph1Δ are described.

Global Analysis: Temperature-Dependent Signals. A sequential model was applied to both

WT Cph1Δ and Y_{176}H Cph1Δ (termed WT and YH, respectively, henceforth) (Figs. S3A-C and S3G-I, respectively), with adequate fit to the data. This approach estimates the underlying "*apparent*" (i.e., experimentally observed) timescales in the data, but does not decompose the *apparent* dynamics into the *microscopic* dynamics describing the evolution of constituent populations. Nevertheless, the sequential EADS can be analyzed to extract useful information such as the Lumi-R formation phase in multi-exponential dynamics[5, 6] and supplies *a priori* information for target model construction. The WT needed six components (Fig. S3A-C) to adequately fit the data (Fig. 3A) and YH needed four components (Fig. S4I-L) for all probed three temperatures (Fig. 3C). Henceforth, EADS from WT will be termed wtEADS and from YH as yhEADS.

For WT, the first component wtEADS1 has fast 120-fs decay time, which is temperature independent. Therefore, this fast component is postulated to be a barrierless early decay on Franck-Condon (FC) region of excited-state potential energy surface to the relaxed excited-state population. This fast dynamics is analogous to early excited-state components observed in femtosecond stimulated Raman experiment on WT.[7] The subsequent wtEADS's (wtEADS2 and wtEADS3, Fig. S3A-C) are temperature dependent as the amplitude between 525 and 720 nm is greater for 8 °C measurement than 25 °C and then for 40 °C (Fig. S4B). By wtEADS4, the temperature-dependent signals become congruent different except for 590 nm to 620 nm region where 40 °C measurement shows more pronounced negative signals (Fig. S4C).

For YH, the yhEADS1 has fast 120-fs decay time constant that is also temperature independent (Fig. S4I), which, like in WT, is postulated to be early FC excited-state relaxations. The yhEADS at different temperatures are compared (Fig. S4I-L). Unlike wtEADS's, the yhEADS's maintain comparable spectral shapes in time that are spectrally near identical to

wtCph1Δ's slow wtEADS4 and wtEADS5 (Fig. S4C, only wtEADS4 shown). The last component, yhEADS4, has lifetime of 1.5 ns to 1.75 ns depending on temperature (Fig. S4L). yhEADS4's spectral shape is near identical to other yhEADS's and thus represent excited-state signals. The Lumi-R-like isomerized photoproduct was not resolved in YH experiments here (Fig. S2J-L).

The wtEADS1 to wtEADS5 are normalized at 440 nm to 530 nm region where ESA band is reasonably clean from bleach and SE contributions; these normalized wtEADS are compared (Fig. S3D-F). Normalized wtEADS1 to wtEADS5 overlap well in 440 nm to 530 nm region and varies in other spectral region. The differences of normalized wtEADS "in sequence" such as normalized wtEADS2 – normalized wtEADS1 are compared (Fig. S3G-I). This allows elucidation of spectral evolution of the forward dynamics that is independent from the excited-state decay, assuming that the relative ESA at 440 nm to 530 nm is strictly correlated with P_r*. Such analysis helped elucidating useful *a priori* for target model construction such as Lumi-R formation time scale in related CBCR NpR6012g4.[6]

The difference between normalized wtEADS1 and wtEADS2 for all three temperatures (Fig. S3G-I, black curves) show small positive amplitude at 575 nm to 620 nm region and a broad negative feature peaking at ~675 nm, which indicates change in SE band amplitude in fast relaxation. The difference between normalized wtEADS2 and wtEADS3 for all three temperatures (Fig. S3G-I, red curves) shows a small positive amplitude peaking around 705 nm. This positive amplitude change in the region can arise from Lumi-R primary photoproduct formation, ground-state intermediate (GSI) formation, which is further characterized by pump-dump-probe experiment,[8] or the red-shifting of SE band from vibrational relaxation. Comparison with Lumi-R spectrum (Fig. S3G-I, magenta circles) shows that the spectral evolution between

wtEADS2 and wtEADS3 is not likely the formation of Lumi-R. The 1.7-ps to 2.7-ps timescale supports vibrational relaxation for the spectral evolution.

The most notable changes occur from difference of normalized wtEADS3 and wtEADS4 and that of normalized wtEADS4 and wtEADS5 (Fig. S3G-I, blue and green curves, respectively). The change from wtEADS3 to wtEADS4 (blue curves) is further explored by comparing with YH signals, where wtEADS4 is replaced with yhEADS2 and difference spectra are deduced with wtEADS3. The two difference spectra overlap remarkably well (Fig. S3G-I, blue curves and orange circles, respectively), indicating that yhEADS2 and wtEADS4 are spectrally identical for all temperature range. This is consistent with similar spectral shape observed for wtEADS4 and wtEADS5 (Fig. S3D-F) to yhEADS (Fig. S4I-L). The difference between normalized wtEADS4 and wtEADS5 are compared with Lumi-R spectrum to show good overlap (Fig. S3G-I, dark cyan curve and magenta circles, respectively). Thus spectral evolution between wtEADS4 and wtEADS5 is Lumi-R formation (i.e., Z-to-E isomerization reaction) with timescale of 50 to 100 ps that is slower than various reported value of 3 ps,[7, 9, 10] ~15 ps,[11] and 30-50 ps.[12]

Based on sequential analysis above, and with additional information from literature such as $\Phi_{\text{Lumi-R}} \approx 15$ %,[13] discrepancy between WT absorbance and fluorescent excitation band,[14] temperature dependence of WT absorbance band,[15] evidence of WT ground state heterogeneity from solid state NMR,[16] the integrated and self-consistent target model is constructed (Fig. 5). Here are some key features of the model and validations:

1. The ground-state heterogeneity (i.e., "photoactive" vs. "fluorescent" subpopulations) (Fig. 5, enclosed in red and blue rectangles, respectively) in thermal equilibrium explains the WT's apparent inverted Arrhenius kinetics (Fig. 3A). The "fluorescent" population is

both spectrally and kinetically analogous to YH evidenced from global sequential analysis (Fig. S3G-I), which has significantly slower excited-state kinetics than WT (Fig. S4). At higher temperature, more "fluorescent" population is occupied (Fig. 5) to slow down the apparent excited-state kinetics and vise versa for the lower temperatures. However each subpopulation (i.e., P_r 1, P_r 2) obeys Arrhenius kinetics with faster excited-state decay at higher temperature. Thus inverted Arrhenius dynamics of WT is phenomenological. The fast FC P_r* are temperature independent at 120-fs for all five subpopulations.

2. Only P_r 2 is the "true" photoactive by generating Lumi-R (Fig. 5). P_r 1 and P_r 2, however, are assumed to share the same excited-state spectra such as SADS of FC P_r* 1 and 2 and the Relaxed P_r* 1 and 2 are the same (Figs. S4E and F, respectively). Similar observation was made for PCB-binding CBCR NpR6012g4 where the excited-state spectra with different lifetime and Lumi-R productivity showed very similar excited-state spectra.[6]
3. The SADS of "fluorescent populations", i.e. FC P_r* 3, 4, 5 and Relaxed P_r* 3, 4, 5 (Fig. 5), are assumed to be spectrally identical (Fig, S4G). The SADS: Fluorescent overlaps well with wtEADS4 (Fig. S4C), consistent with sequential EADS analysis (Fig. S3G-I). The SADS: Fluorescent also compares well with yhEADS's, except for the 120-fs fast yhEADS1 where SADS overestimates 630 nm to 750 nm region (Fig. S4I-L). Due to yhEADS1's fast relaxation, this assumption does not adversely affect our spectral analysis. This demonstrates that the WT fluorescent population is spectrally analogous to YH dynamics.
4. The fluorescent populations (Fig. 5, P_r 3-5) have the same excited-state lifetime as YH for respective temperatures (Fig. S4.I-L). This makes WT fluorescent population and YH

both spectrally and temporally analogous to each other.

5. The $\Phi_{Lumi\text{-}R}$ is set at ~15 % based on previous estimation.[13] There is a slight variation of $\Phi_{Lumi\text{-}R}$ with 13.8, 14.3 and 13.7 % at 8, 25, and 40 °C, respectively (Fig. S7A-C). Comparable $\Phi_{Lumi\text{-}R}$ at 40 °C to 8 °C and 25 °C is unexpected given that it contains less "photoactive" populations (see #1 above). This discrepancy is reconciled by 40 °C having higher efficiency in generating Lumi-R, which also has faster excited-state lifetime (Fig. 5).
6. SADS of each spectral category are temperature independent (Fig. S4E-H) unlike EADS (Fig. S4A-D). This supports that temperature-dependent signals originating from different occupancy of "photoactive" and "fluorescent" populations with respective temperature-independent spectra.
7. The 570 nm to 630 nm region is spectrally sensitive to heterogeneity in Cph1Δ. The "photoactive" population exhibits positive amplitude in that region and "fluorescent" population exhibits negative amplitude (Fig S4F and G, respectively). The 605-nm kinetic traces (Fig. S2F) show that 40 °C has lesser initial amplitude and greater negative amplitude once the "photoactive" population decays, to be consistent with the heterogeneity hypothesis. Similar result is also observed in excitation-dependent studies on Cph1Δ in this study and also the study by van Thor and coworkers, which reported more pronounced negative amplitude in the 570 to 630-nm region at higher energy excitation.[9]

Global Analysis: Excitation-Wavelength-Dependent Signals. The target model for the DEWI-PP signals (Fig. S5) are adapted from 25 °C integrated model (Fig. 5) with the same connectivity

scheme and time constants for each constituent population. Only difference is the excitation-wavelength-dependent P_r* occupation differences, where 600-nm and 670-nm excitation generated 52 % and 75 % of photoactive populations, respectively, with Lumi-R generating P_r 2* at 32 % and 40 %. This explains excitation-wavelength-dependent P_r* kinetics (Fig. 4B) and $\Phi_{Lumi\text{-}R}$ (Figs. 4D and S7D).

The WT EADS and SADS are compared (Figs. S6A-D and E-H, respectively). The discrepancy between 600-nm and 670-nm excitation WT signals in EADS (also emphasized in Fig. S5B and C) is diminished in SADS. Unlike temperature-dependent signals, however, which demonstrates temperature-independent SADS, the WT SADS from DEWI-PP signals still shows excitation-wavelength dependence. The YH DEWI-PP signals (Fig. S5G-L) also shows the excitation-wavelength dependent spectra unlike the temperature-dependent signals (Fig. S2J-L). The SADS of fluorescent populations from WT DEWI-PP signals are compared with YH EADS (Fig. S6I-L) to show that SADS (dark cyan and gray curves for 600-nm and 670-nm excitation signals, respectively) matches qualitatively well to the YH EADS (blue and red curves, respectively). Thus it is likely that the signals include intrinsic excitation-wavelength dependence in spectra that is independent from the initial P_r* occupation difference caused by 600-nm and 670-nm excitation pulses.[17] The Lumi-R SADS shows the same magnitude between 600-nm and 670-nm excitation signals (Fig. S6H) to justify excitation-wavelength-dependent $\Phi_{Lumi\text{-}R}$ (Fig. S7D).

References

1. Holzwarth, A. R. (1996) Data Analysis of Time-Resolved Measurements, In *Biophysical techniques in photosynthesis* (Amesz, J., and Hoff, A. J., Eds.), pp 75-92, Springer, Netherlands.
2. van Stokkum, I. H. M., Larsen, D. S., and van Grondelle, R. (2004) Global and target analysis of time-resolved spectra, *Biochimica Et Biophysica Acta-Bioenergetics 1657*, 82-104.
3. Kim, P. W., Pan, J., Rockwell, N. C., Chang, C.-W., Taylor, K. C., Lagarias, J. C., and Larsen, D. S. (2012) Ultrafast E to Z Photoisomerization Dynamics of the Cph1Δ Phytochrome, *Chemical Physics Letters 549*, 86-92.
4. Kim, P. W., Freer, L. H., Rockwell, N. C., Martin, S. S., Lagarias, J. C., and Larsen, D. S. (2012) Second-Chance Forward Isomerization Dynamics of the Red/Green Cyanobacteriochrome NpR6012g4 from Nostoc punctiforme, *Journal of the American Chemical Society 134*, 130-133.
5. Kim, P. W., Freer, L. H., Rockwell, N. C., Martin, S. S., Lagarias, J. C., and Larsen, D. S. (2012) Femtosecond Photodynamics of the Red/Green Cyanobacteriochrome NpR6012g4 from Nostoc punctiforme. 2. Reverse Dynamics, *Biochemistry 51*, 619-630.
6. Kim, P. W., Freer, L. H., Rockwell, N. C., Martin, S. S., Lagarias, J. C., and Larsen, D. S. (2012) Femtosecond Photodynamics of the Red/Green Cyanobacteriochrome NpR6012g4 from Nostoc punctiforme. 1. Forward Dynamics, *Biochemistry 51*, 608-618.
7. Dasgupta, J., Frontiera, R. R., Taylor, K. C., Lagarias, J. C., and Mathies, R. A. (2009) Ultrafast excited-state isomerization in phytochrome revealed by femtosecond stimulated Raman spectroscopy, *Proceedings of the National Academy of Sciences of the United States of America 106*, 1784-1789.
8. Freer, L. H., Kim, P. W., Corley, S. C., Rockwell, N. C., Zhao, L., Thibert, A. J., Lagarias, J. C., and Larsen, D. S. (2012) Chemical Inhomogeneity in the Ultrafast Dynamics of the DXCF Cyanobacteriochrome Tlr0924, *Journal of Physical Chemistry B 116*, 10571-10581.
9. Fitzpatrick, A. E., Lincoln, C. N., van Wilderen, L. J., and van Thor, J. J. (2012) Pump-Dump-Probe and Pump-Repump-Probe Ultrafast Spectroscopy Resolves Cross Section of an Early Ground State Intermediate and Stimulated Emission in the Photoreactions of the Pr Ground State of the Cyanobacterial Phytochrome Cph1Δ, *The journal of physical chemistry. B 116*, 1077-1088.
10. van Wilderen, L., Clark, I. P., Towrie, M., and van Thor, J. J. (2009) Mid-Infrared Picosecond Pump-Dump-Probe and Pump-Repump-Probe Experiments to Resolve a Ground-State Intermediate in Cyanobacterial Phytochrome Cph1Δ, *Journal of Physical Chemistry B 113*, 16354-16364.
11. Heyne, K., Herbst, J., Stehlik, D., Esteban, B., Lamparter, T., Hughes, J., and Diller, R. (2002) Ultrafast dynamics of phytochrome from the cyanobacterium Synechocystis, reconstituted with phycocyanobilin and phycoerythrobilin, *Biophysical Journal 82*, 1004-1016.
12. Yang, Y., Linke, M., von Haimberger, T., Hahn, J., Matute, R., Gonzalez, L., Schmieder, P., and Heyne, K. (2012) Real-Time Tracking of Phytochrome's Orientational Changes During Pr Photoisomerization, *Journal of the American Chemical Society 134*, 1408-1411.
13. Lamparter, T., Mittmann, F., Gartner, W., Borner, T., Hartmann, E., and Hughes, J. (1997) Characterization of recombinant phytochrome from the cyanobacterium Synechocystis, *Proceedings of the National Academy of Sciences of the United States of America 94*, 11792-11797.
14. Mailliet, J., Psakis, G., Feilke, K., Sineshchekov, V., Essen, L.-O., and Hughes, J. (2011) Spectroscopy and a High-Resolution Crystal Structure of Tyr263 Mutants of Cyanobacterial Phytochrome Cph1Δ, *Journal of Molecular Biology 413*, 115-127.

15. Spillane, K. M., Dasgupta, J., Lagarias, J. C., and Mathies, R. A. (2009) Homogeneity of Phytochrome Cph1Δ Vibronic Absorption Revealed by Resonance Raman Intensity Analysis, *Journal of the American Chemical Society 131*, 13946-13948.
16. Song, C., Psakis, G., Lang, C., Mailliet, J., Gartner, W., Hughes, J., and Matysik, J. (2011) Two Ground State Isoforms and a Chromophore D-Ring Photoflip Triggering Extensive Intramolecular Changes in a Canonical Phytochrome, *Proceedings of the National Academy of Sciences of the United States of America 108*, 3842-3847.
17. Demchenko, A. P. (2002) The red-edge effects: 30 years of exploration, *Luminescence 17*, 19-42.

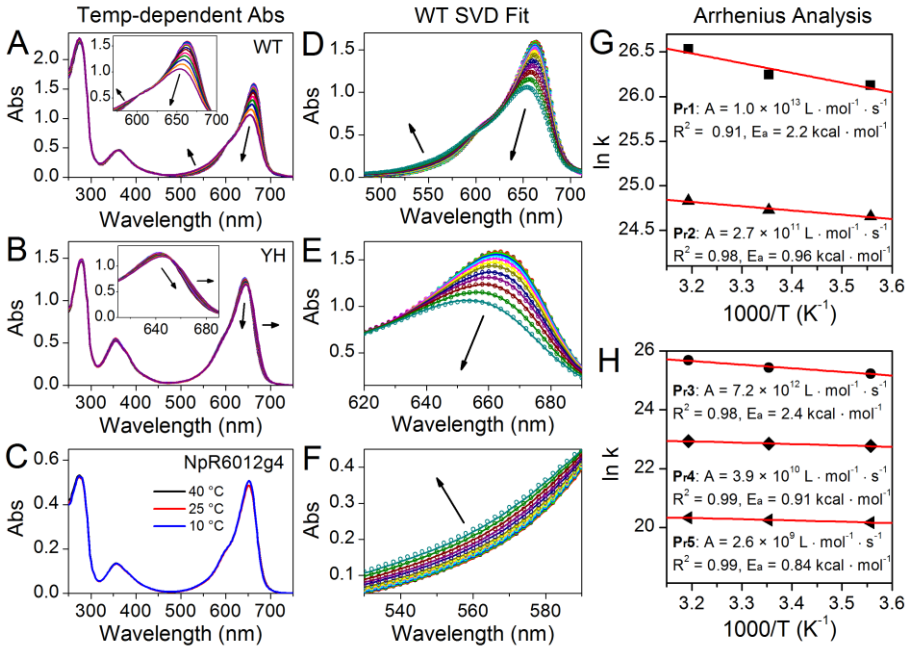

Figure S1. (A-C) Temperature-dependent absorption of WT, YH, and cyanobacteriochrome NpR6012g4. For WT and $Y_{176}H$, absorption bands from 7 to 43 °C with 3 °C intervals are measured and plotted with arrows indicating direction of increase of temperature. (D-F) SVD analysis fit (curves) to the WT temperature-dependent absorption bands (symbols). Panel E and F zoom in at different spectral regions for better visual inspection. (G, H) Arrhenius analysis based on the integrated model (Fig. 5). The relaxed excited state for each subpopulation, P_r1 – P_r5, is represented, with Panel G representing "photoactive" population and Panel H representing "fluorescent" populations. The activation barrier, E_a, has unit of kcal · mol^{-1}. The pre-exponential coefficient, A, has unit of L · mol^{-1} · s^{-1}.

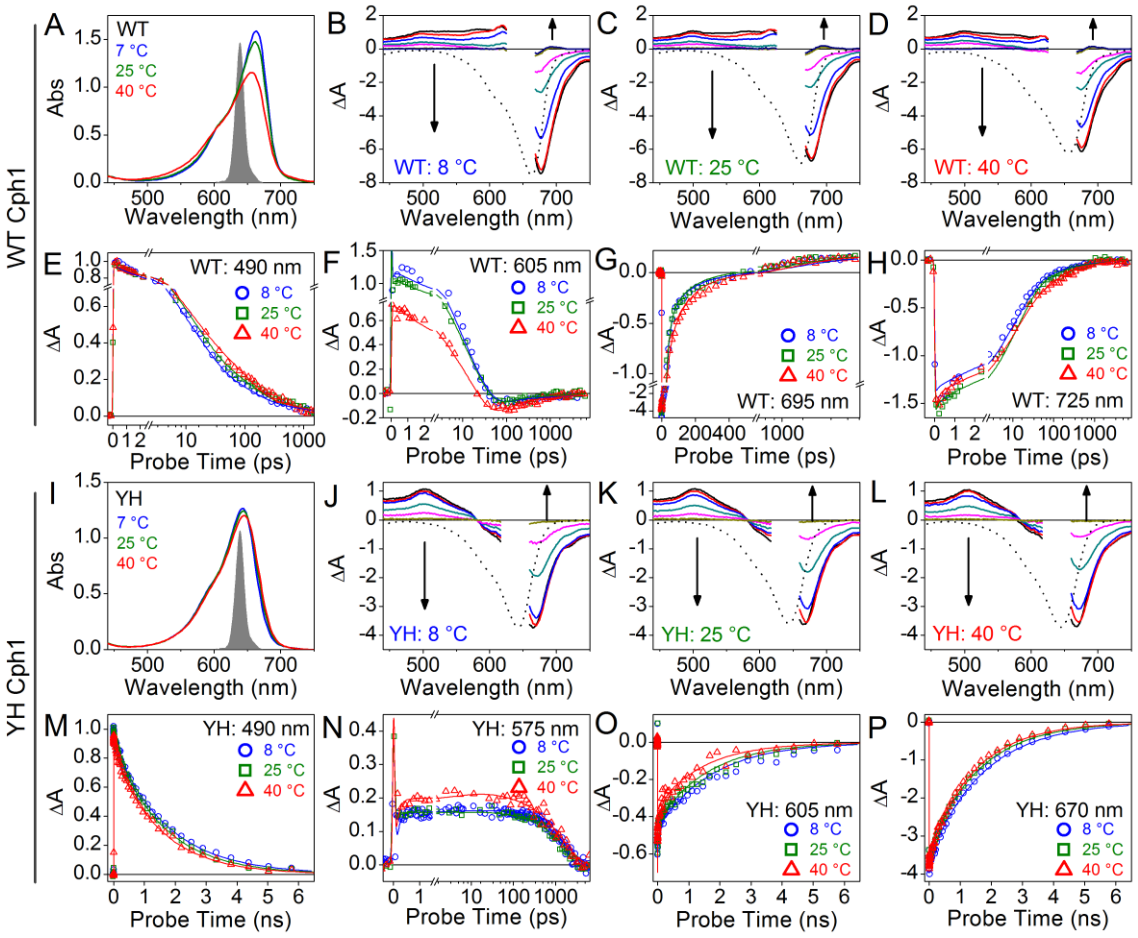

Figure S2. Raw data of temperature-dependent experiments for WT (A-H) and YH (I-P). (A, I) Absorbance band at 7, 25, and 40 °C for WT and YH, respectively, overlaid with 630-nm pump spectrum. (B-D) WT transient spectra at probe time 180 fs, 1 ps, 5 ps, 22 ps, 52 ps, 1 ns, and 6 ns in direction of arrows, overlaid with inverted absorption band (black dash) at respective temperature. All panels have axis identical in scale for temperature-dependent amplitude comparison. (E-H) WT kinetic traces (symbols) at selected probe wavelengths fitted with the integrated model (Fig. 5, curves). (J-L) YH transient spectra at probe time 1 ps, 52 ps, 205 ps, 1 ns, 2.5 ns, and 6 ns in direction of arrows, overlaid with inverted absorption band (black dash) at respective temperature. All panels have axis identical in scale for temperature-dependent amplitude comparison (M-P) YH kinetic traces (symbols) at selected probe wavelengths fitted with the global sequential model (Fig. S4I-L, curves).

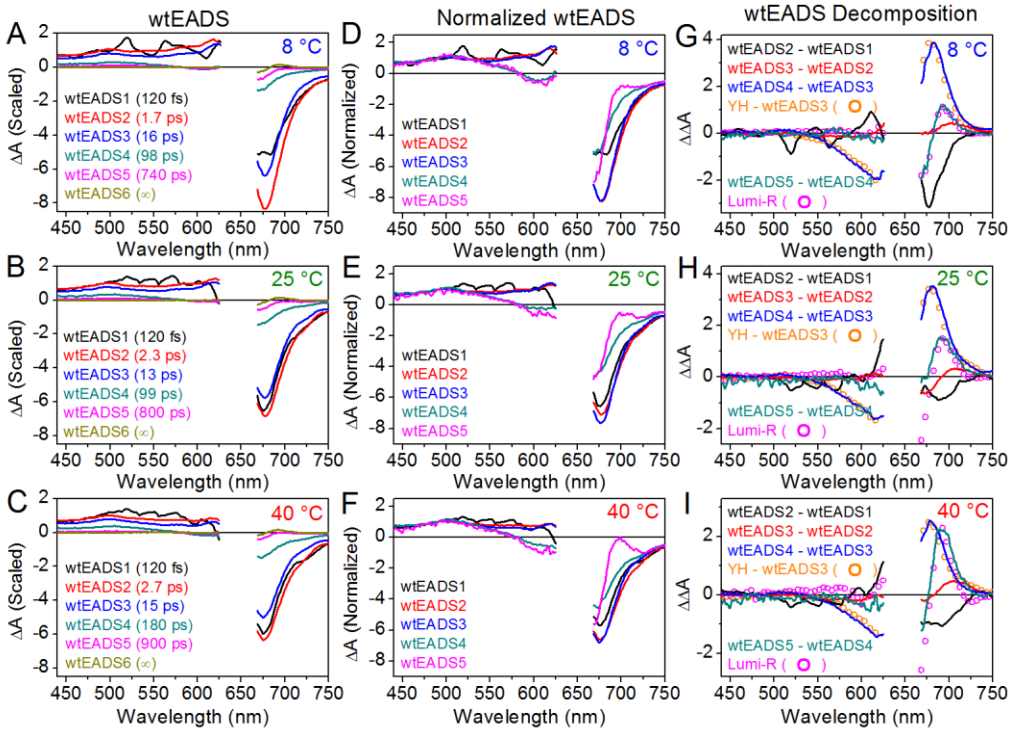

Figure S3. The 6-component sequential global model analysis of temperature-dependent WT signals of respective temperature. (A-C) wtEADS of 8 °C, 25 °C, and 40 °C, respectively. They are scaled by the initial amplitude at 490-nm probe wavelength. (D-F) wtEADS1-5 normalized at 440 nm to 500 nm region for respective temperature. (G-I) Sequential subtraction of the normalized wtEADS from Panel D-F to extract spectral evolution that is independent from the excited-state decay for respective temperatures. wtEADS4 – wtEADS3 difference (blue curve) is compared with YH – wtEADS3 difference (orange circles). YH here is wtEADS4 from YH sequential global analysis (Fig. S4L). wtEADS5 – wtEADS4 difference (dark cyan curve) is compared with Lumi-R (magenta circles, Figure 3D), which is represented by wtEADS6 from Panel A-C (dark yellow curves) for respective temperatures.

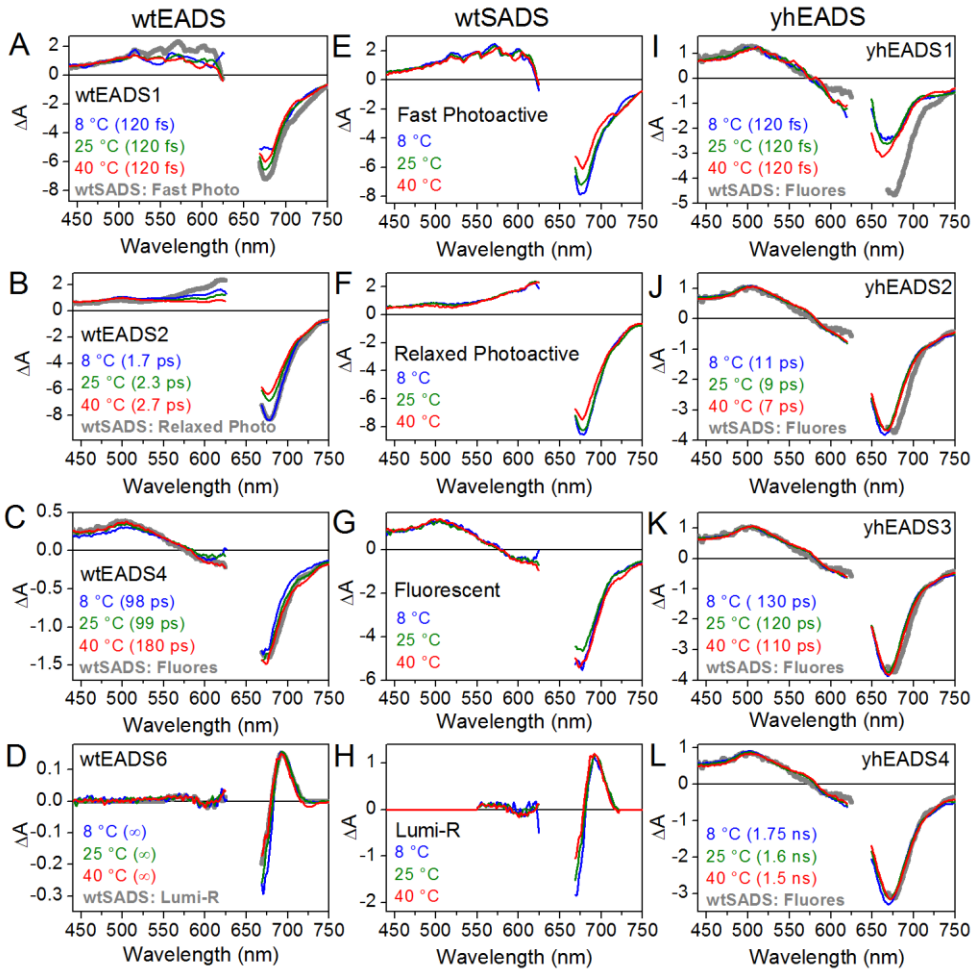

Figure S4. Comparison of wtEADS, wtSADS, and yhEADS to illustrate consistency in the integrated model (Fig. 5). (A-D) wtEADS1, 2, 4, and 6, respectively. Each panel compares wtEADS from respective temperatures and they are overlaid with the respectively time-scaled wtSADS from Panel E-H (25 °C, thick grey curves) for comparison. (E-H) wtSADS extracted from the integrated model (Fig. 5). Each panel compares wtSADS from respective temperatures. (I-L) yhEADS 4-component sequential global analysis. Each panel compares yhEADS from respective temperatures and they are overlaid with the fluorescent wtSADS from Panel G (25 °C, thick grey curves) for comparison.

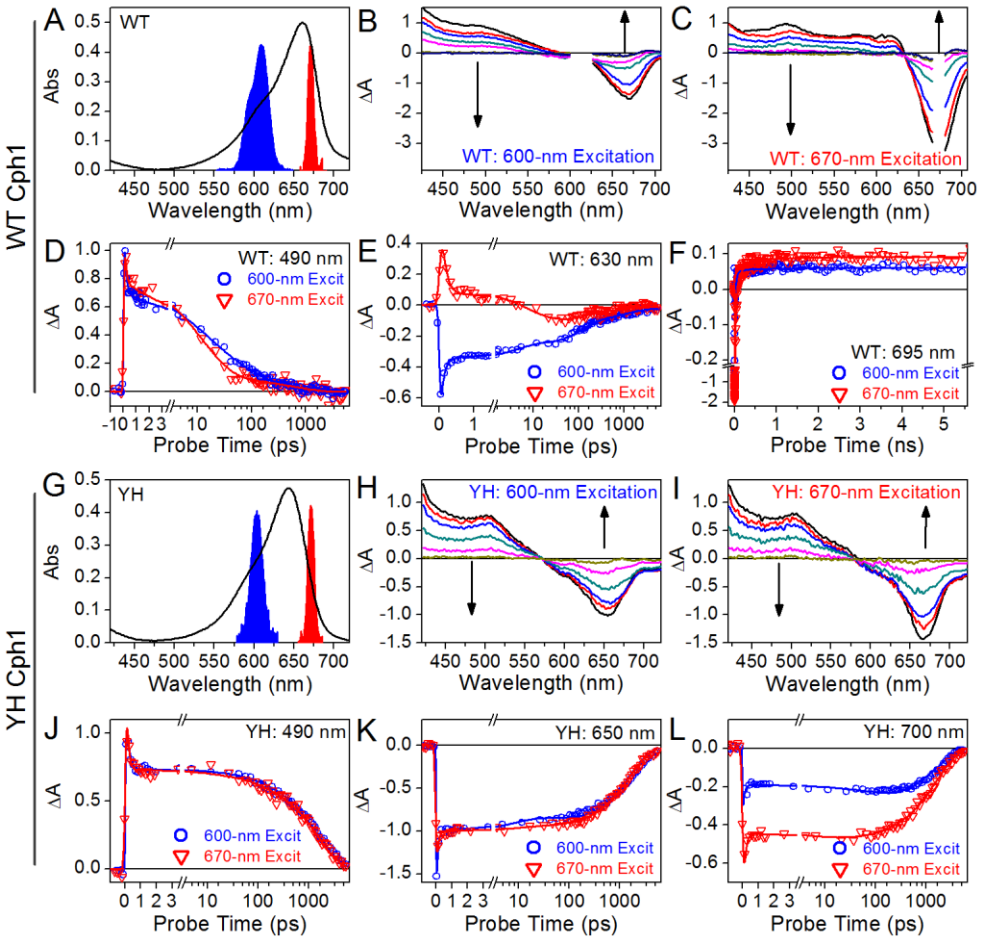

Figure S5. The raw data of DEWI-PP (double-excitation-wavelength-interleaved pump-probe experiment) of WT (A-F) and YH (G-L). (A, G) Absorbance band at 25 °C for WT and YH, respectively, overlaid with 600-nm and 670-nm pump spectra (blue and red, respectively). (B, C) WT transient spectra at probe time 210 fs, 1 ps, 5 ps, 22 ps, 52 ps, 1 ns, and 5.6 ns in direction of arrows for 600-nm and 670-nm excitation, respectively. The panels have axis identical in scale for excitation-dependent amplitude comparison. (D-F) WT kinetic traces (symbols) at selected probe wavelengths fitted with the sequential model (Fig. S6A-D, curves). (H, I) YH transient spectra at probe time 1 ps, 52 ps, 203 ps, 1 ns, 2.5 ns, and 5.6 ns in direction of arrows for 600-nm and 670-nm excitation, respectively. The panels have axis identical in scale for excitation-dependent amplitude comparison. (J-L) YH kinetic traces (symbols) at selected probe wavelengths fitted with the global sequential model (Fig. S6I-L, curves).

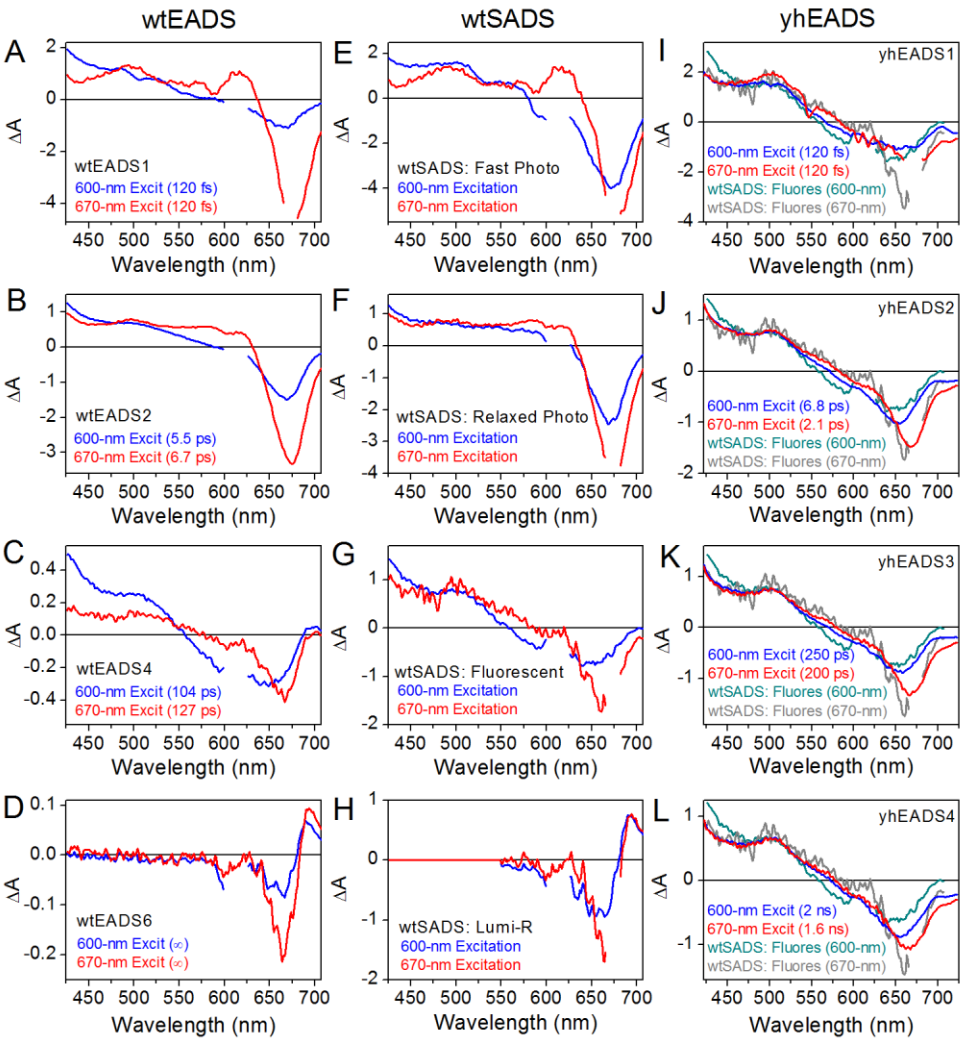

Figure S6. Comparison of DEWI-PP wtEADS, wtSADS, and yhEADS to illustrate consistency with the integrated model (Fig. 5). (A-D) wtEADS1, 2, 4, and 6, respectively. Each panel compares wtEADS from respective excitation-wavelength conditions. (E-H) wtSADS extracted from the integrated model (Fig. 5). Each panel compares wtSADS from respective excitation-wavelength conditions. (I-L) yhEADS 4-component sequential global analysis. Each panel compares yhEADS from respective excitation-wavelength conditions and they are overlaid with the fluorescent wtSADS from Panel G (light grey and dark grey curves from 600-nm and 670-nm excitations, respectively) for comparison.

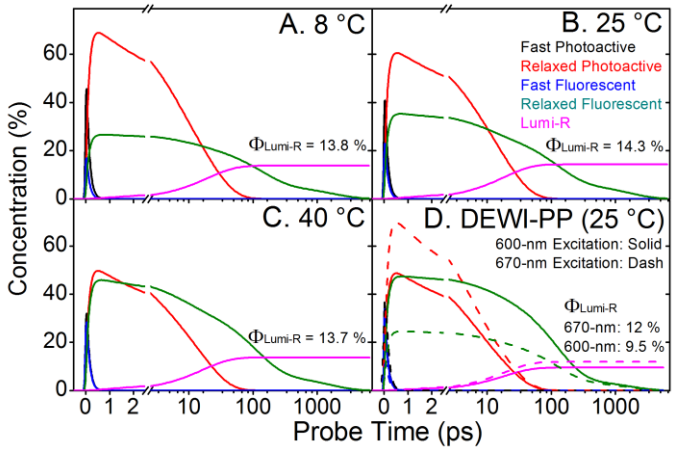

Figure S7. The concentration profile of temperature-dependent studies (A-C) and DEWI-PP (D).